

Combined Optical Connectivity and Optical Flow Velocimetry for measurement of the interfacial velocity of a liquid jet in gas cross-flow

Tianyi Wang* and Yannis Hardalupas

Imperial College London, Mechanical Engineering Department, London SW7 2AZ, UK

* Correspondent author: tw5017@ic.ac.uk

Keywords: Optical Connectivity, Optical Flow Velocimetry, Interfacial motion, Liquid jet in crossflow, Atomisation

ABSTRACT

Liquid jet in crossflow (LJIC) is a process in which a high-speed gas crossflow deforms and shears a continuous liquid flow into tiny droplets. This study quantifies the liquid surface motion of LJIC during the primary breakup process, which has not been fully assessed due to limited optical access close to the nozzle exit. The interfacial velocity of a breaking liquid jet indicates the interaction of the gas and liquid flows and the initial velocity of the stripped droplets. However, the local interfacial liquid velocities have not been measured, since no measurement technique is available, and they have only been estimated from theoretical and computational studies. Optical Connectivity (OC) is a new optical technique, which introduces a laser beam through an atomiser nozzle and relies on total internal reflection at the liquid interface to propagate the laser light inside the continuous liquid. This allows the recording of the instantaneous features of the disintegrating continuous liquid and its interface during the primary atomisation at the near nozzle region through imaging of the emitted fluorescent intensity from the liquid flow. The current research reports time-dependent OC measurements of the temporal evolution of the liquid interface structures along a LJIC. The LJIC breakup behaviour is reported for different atomisation regimes, as determined by non-dimensional parameters. Optical Connectivity is combined with Optical Flow Velocimetry (OFV) to quantify the local interfacial liquid velocities of liquid interface structures of the LJIC for a range of gas Weber numbers between 14.9 - 112.6 and liquid-to-gas momentum ratios between 2.1 - 36.4. The combined OC-OFV measurements report the spatial distribution of interfacial velocities along the surface of LJIC and reveal the physics of the contribution of gaseous shear and liquid jet geometry on the atomisation process.

1. Introduction

A liquid stream injected into high-speed gaseous crossflow, referred as a liquid jet in crossflow (LJIC), has been studied for several applications, such as blade cooling system, agriculture spray and fuel atomisation in combustors (Ghosh & Hunt, 1998; Mahesh, 2013; Wu, Kirkendall, Fuller, & Nejad, 1997). For liquid-fuel combustion devices, LJIC has been utilized to potentially enhance combustion efficiency and reduce pollutant emissions due to the characteristics of the atomisation mechanism of LJIC. A more controllable penetration and distribution of the stripped-off fuel droplets from the liquid jet can be achieved by carefully adjusting the relevant parameters, while a uniform air-fuel mixture ratio is also generated by LJIC, owing to the complex gas flow structures

surrounding the injected liquid jet such as counter-rotating vortex pair (CVP) (Behzad, Ashgriz, & Karney, 2016; Elshamy, Tambe, Cai, & Jeng, 2006; Kelso, Lim, & Perry, 1996; Li & Soteriou, 2016, 2018; Eugene Lubarsky, Reichel, Zinn, & McAmis, 2010; Wu, Kirkendall, Fuller, & Nejad, 1998). However, the physics of the primary breakup stage are still not fully understood, particularly for the region close to the nozzle exit. A detailed study of the primary breakup of LJIC, including the characteristics of the disintegrating features and interfacial motion of the liquid jet, is required since it is connected to fuel droplet formation, the resulting droplet sizes and spatial distribution of the spray in the combustor.

The main challenge of accurately describing the primary breakup of LJIC is the dense droplet clouds surrounding the liquid core which limit the visualization of the breakup features and the detailed geometry of the continuous liquid core, especially at the multimode and shear breakup regime where the surface breakup dominates the entire jet. At the near region of the primary breakup, the gas flow vortex structures may destabilise the liquid surface and cause breakup and also carry droplets upstream of the liquid jet region, as measured by Particle Image Velocimetry (PIV) and Phase Doppler Particle Analyser (PDPA) and demonstrated by simulations (Behzad et al., 2016; Elshamy et al., 2006; Li & Soteriou, 2016; Eugene Lubarsky et al., 2010). However, such measurements were only performed further away from the breakup region where the liquid concentration is reduced. Shadowgraphic techniques have been used to visualise the liquid breakup region, but can only capture the breakup characteristics of liquid jets with less complex breakup features, such as those present under column and bag breakup regimes. Meanwhile, when the liquid jet break regimes cause higher optical depth, the corresponding breakup features, such as breakup length and liquid penetration trajectory, can vary significantly (Mohsen Broumand & Birouk, 2016).

To subside the optical attenuation of light and multiple scattering effects of the dense droplet clouds around the breakup region, which limit shadowgraphic visualisations, ballistic imaging was developed to observe the breakup region at the near-field of atomisers (Linne, Paciaroni, Gord, & Meyer, 2005). Nevertheless, this method has not been applied extensively to study the breakup process physics under realistic atomisation conditions. Recently, Optical Connectivity (OC) was proposed by Charalampous et al. (2007) to avoid or limit the influence from the surrounding droplets in order to study the breakup physics of air-assisted atomisation. Besides, Wang and Hardalupas (2021) have combined the Optical Flow Velocimetry (OFV) and Optical Connectivity (OC) [OC-OFV], to quantify the interfacial velocity along the surface of a continuous liquid jet injected by a pressure jet atomiser into quiescent air. This technique measured the

detailed distribution of interfacial velocities on the liquid surface and revealed the significance of liquid viscosity and liquid shear layer on atomisation process.

The current study applies both OC and shadowgraphy to study the breakup features during primary breakup of LJIC and compares the results from both techniques for three breakup regimes, namely bag breakup, multimode breakup and shear breakup, which are defined in the next section. Then, the optical flow velocimetry (OFV) is combined with OC to measure the local interfacial liquid velocities of liquid interface structures of the LJIC. This provides new information of breakup and interfacial features of LJIC in the near-field region.

2. Experiment set-up and methodology

2.1 Spray facility and flow conditions

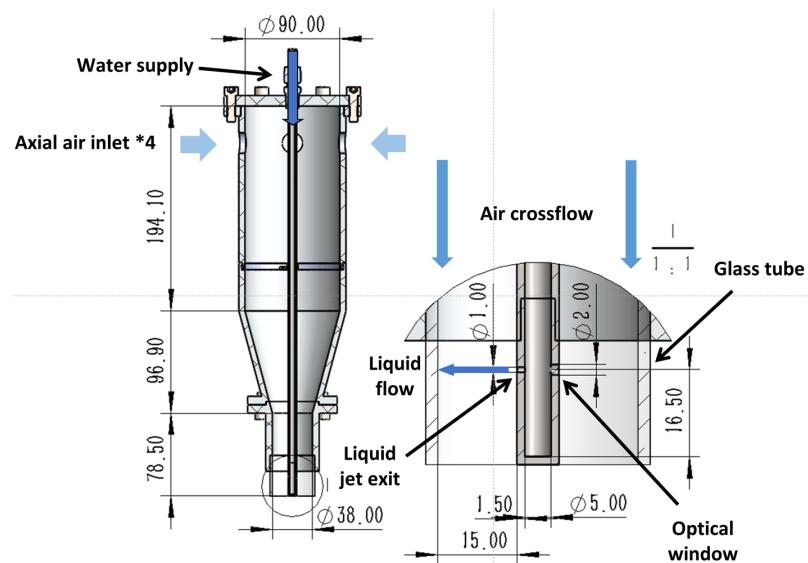


Fig. 1: Schematic of atomizer of liquid jet exposed to a cross stream of air (elevation view). Detail at bottom right shows design of liquid nozzle exit and optical window.

The specially designed gas crossflow atomiser used in the current study is presented in **Fig. 1**, which allows the application of optical connectivity (OC) and shadowgraphy techniques. The main body of the atomiser was set vertically and designed with four axial inlets which are mounted at the far end of a cylindrical plenum chamber to allow the gas flow supply to the nozzle after flowing through a mounted straighter. A more detailed description of the atomiser can be found in Hadjiyiannis (2014). The cylindrical chamber with diameter 90 mm was closed at the far end by a plate and, at the other side, was connected to a conical contraction with 38 mm exit diameter to accelerate the gas flow. The contraction ended in a straight nozzle and was extended by a straight glass tube, which was used to confine the gas flow from the contraction exit.

Moreover, the glass tube allowed the light source of optical techniques to illuminate the gas and liquid flow. It is within the length of the glass tube that the atomisation of the injected liquid jet takes place and can be studied, while the surrounding air flow velocity remains constant.

The liquid was supplied through a long straight stainless-steel tube of circular cross-section with 5mm internal and 8mm external diameter (more detail in **Fig. 1**). The delivering tube was supported along the centreline of the atomiser main body and was connected to the liquid supply at one end. The other end of the delivering tube was closed and a circular hole with diameter of 1mm was drilled at the side of the tube normal to its centreline at the start of the transparent glass tube. In this way, a liquid jet could be injected normally to the gas flow within the bounds of the transparent glass tube, which allows the study for LJIC. Therefore, the L/D value of the injecting nozzle is 1.5, while the annular gap between the central liquid-delivering tube and the outer glass tube was 15mm. For the implementation of the optical connectivity technique, an optical window was placed on the liquid-delivering tube right opposite of the liquid exit, as shown in the detail at the bottom right of **Fig. 1**. The transparent glass tube of the gas flow annulus provided direct optical access to the optical window at the back of the liquid injection orifice. A laser beam could therefore be directed into the liquid jet in order to apply the OC technique. In the current study, Rhodamine B was mixed in the supplied water with concentration of 5×10^{-7} mol/L and injected into the high-speed air crossflow through the 1mm diameter orifice. The LED light source of shadowgraphy technique, at the same time, can also illuminate the studied field through the transparent glass tube. The air and liquid flow rates are controlled by rotameters.

Tab. 1: Properties of gas and liquid fluids.

$\rho_G (\text{kg/m}^3)$	$\rho_L (\text{kg/m}^3)$	$\mu_L (\text{pa} \cdot \text{s})$	$\mu_G (\text{pa} \cdot \text{s})$	$\sigma (\text{N/m})$
1.225	997	8.90×10^{-4}	1.85×10^{-5}	7.28×10^{-2}

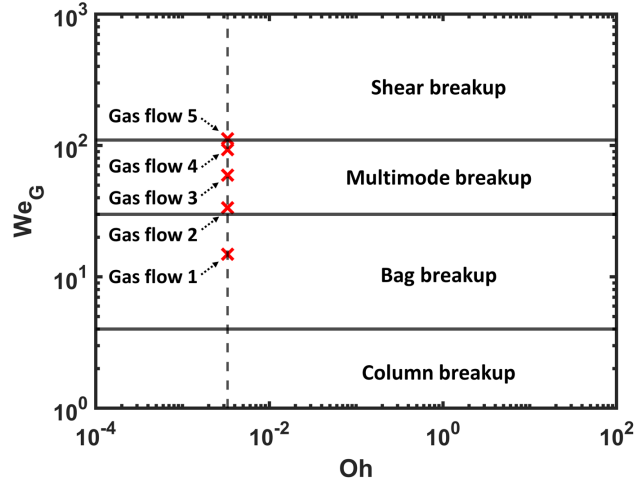


Fig. 2: Breakup regime map of LJIC suggested by Sallam et al. (2004).

Several non-dimensional parameters can affect the characteristics of the cross-flow atomisation, such as breakup regimes, droplet size distribution and liquid breakup length (Mazallon, Dai, & Faeth, 1999; Ng, Sankarakrishnan, & Sallam, 2008; Sallam et al., 2004; Wu et al., 1997). The considered non-dimensional parameters include: (i) gas Weber number $We_G = \rho_G V_G^2 D / \sigma$, (ii) liquid-to-gas momentum flux ratio $M = \rho_L U_L^2 / \rho_G V_G^2$, (iii) Ohnesorge number $Oh = \mu_L / \sqrt{\rho_L D \sigma}$, (iv) gas Reynolds number $Re_G = \rho_G V_G D / \mu_G$ and (v) liquid Reynolds number $Re_L = \rho_L U_L D / \mu_L$. These parameters have been reported to affect or determine the breakup features of the LJIC (Birouk, Azzopardi, & Stabler, 2003; Mohsen Broumand & Birouk, 2016; M Broumand & Birouk, 2019; Ng et al., 2008; Osta & Sallam, 2007; Sallam et al., 2004; Sallam, Ng, Sankarakrishnan, Aalburg, & Lee, 2006; Wu et al., 1998). The notations are as follows: diameter of the injection orifice D , density of crossflow gas ρ_G , density of injected liquid ρ_L , liquid and gas viscosity μ_L and μ_G , and liquid surface tension σ remain constant, where liquid nozzle diameter D is equal to 1 mm. Therefore, by varying the crossflow gas velocity V_G , the We_G number can be controlled to access different breakup regimes while the liquid velocity U_L is kept constant.

Tab. 2: Non-dimensional parameters of considered flow cases.

Group	U_L (m/s)	Gas Flow No.	V_G (m/s)	We_G	M	Re_G	Re_L	Oh	Breakup Regime
1	4.2	1	29.8	14.9	16.1	1973	4677	3.3×10^{-3}	Bag
		2	44.7	33.6	7.2	2960			Multimode
		3	59.5	59.6	4.1	3940			Multimode
		4	74.4	93.1	2.6	4926			Multimode
		5	81.8	112.6	2.1	5417			Shear
2	5.3	1	29.8	14.9	25.7	1973	5937	3.3×10^{-3}	Bag
		2	44.7	33.6	11.4	2960			Multimode
		3	59.5	59.6	6.5	3940			Multimode
		4	74.4	93.1	4.1	4926			Multimode
		5	81.8	112.6	3.4	5417			Shear

3	6.3	1	29.8	14.9	36.4	1973	7057	Bag
		2	44.7	33.6	16.2	2960		Multimode
		3	59.5	59.6	9.1	3940		Multimode
		4	74.4	93.1	5.8	4926		Multimode
		5	81.8	112.6	4.8	5417		Shear

The breakup regime map suggested by Sallam et al. (2004), given in **Fig. 2**, is used to guide the operating flow conditions and define the breakup regimes. In addition, due to the low value of L/D of the injecting nozzle, the initial injected liquid jet is assumed to be non-turbulent. Five gas flowrates, shown in **Tab. 2**, are considered in the current study and are marked on the regime map of **Fig. 2** to indicate the relevant breakup regime. The first gas flowrate ($V_G=29.8$ m/s) falls in the bag breakup regime ($4 < We_G < 30$) where the breaking bag structures can be clearly observed (E Lubarsky, Shcherbik, Bibik, Gopala, & Zinn, 2012; Ng et al., 2008), and the last gas flowrate with the maximum V_G (gas flow 5) is dominated by strong surface stripping and falls in the shear breakup regime ($We_G > 110$) (Sallam et al., 2004; Wu et al., 1998). The rest three gas flowrates are in the multimode breakup regime ($30 < We_G < 110$) where both the bag breakup and surface stripping coexist, while the competition between bag and surface breakup leads to a breaking jet with more complex features. Moreover, the liquid jet trajectory and maximum penetrating length are mainly influenced by the momentum flux ratio M , which is varied by the gas crossflow velocity V_G and liquid jet velocity U_L . To evaluate the effect of M on the breakup characteristics, three different values of U_L (4.2 m/s, 5.3 m/s and 6.4 m/s) were also studied and all the flow cases are separated into three groups. Each group has flow conditions, where the liquid jet is introduced with a constant U_L , but V_G is varied. In this way, for the same V_G , We_G number is identical for different groups, while the magnitude of M increases from group 1 to group 3. The liquid and gas Reynolds numbers Re_L and Re_G are also considered as influential factors, since the liquid jet turbulence has been suggested that modifies the boundaries of the breakup regimes (Lee, Aalburg, Diez, Faeth, & Sallam, 2007; Sallam, Dai, & Faeth, 2002; Sallam et al., 2006) and the gas flow conditions may also affect the dominant mode of the interfacial instabilities (Arienti & Soteriou, 2009; Li & Soteriou, 2016, 2018; Ng et al., 2008). In addition, the measured breakup characteristics of the different flow cases allow the evaluation of existing theoretical and computational studies. **Tab. 1** and **Tab. 2** list the physical properties of the fluids and the non-dimensional parameters of the considered flow conditions respectively.

2.2 Optical arrangement and coordinate system

Fig. 3(a) shows a plan view of the optical arrangement for carrying out optical connectivity (OC) and shadowgraphy techniques imaging respectively. A nanosecond Nd:YAG laser (New Wave

Research, Solo 120), operating at 532nm wavelength, is used as the illumination source for OC. The typical pulse duration and maximum pulse energy of this laser are 4 ns and 75 mJ. A laser beam with initial 6mm diameter is introduced into the liquid jet nozzle through the optical window after appropriate adjustments by lenses. A LED light source was placed normal to the axis of the liquid jet for shadowgraphy. By separately operating OC and shadowgraphy, the effects of the cloud of the surrounding droplets on the imaging of the primary breakup features could be analysed, while the relevant breakup characteristics can also be quantified by suppressing the influence of surrounding droplets with the OC technique. The side-view images of the disintegrating liquid jet are captured from a PCO Sensicam QE inter-frame CCD camera (12 bit, 1040×1376 pixels) with SIGMA lens with 105 mm focal length and f-number 2.8 (see Fig. 3(a)). Since Rhodamine B which dissolved in water absorbs laser light at 532nm and emit fluorescence with peak wavelength at around 575nm at room temperature (Seuntiëns, Kieft, Rindt, & Van Steenhoven, 2001), a Schott OG 550 long pass optical filter was mounted in front of the lens to remove the illuminating green laser light and any other undesirable light. Fig. 3(b) presents the coordinate system with the elevation view used in the current study. The origin of the coordination system is set at the centre of the liquid jet nozzle exit. Z axis is prescribed to depict the streamwise direction of the liquid jet, which can be used to indicate the penetration distance of the liquid jet from the nozzle exit. Y axis is set along the air crossflow direction, which is perpendicular to X axis. The camera is set along the X axis, while the laser source for OC is guided through the liquid jet along the Z axis and the LED light source is directed along the X axis. The physical dimension of the recorded images is about 8.7 mm x 6.6mm, resulting in a spatial resolution of around 6.3 $\mu\text{m}/\text{pixel}$.

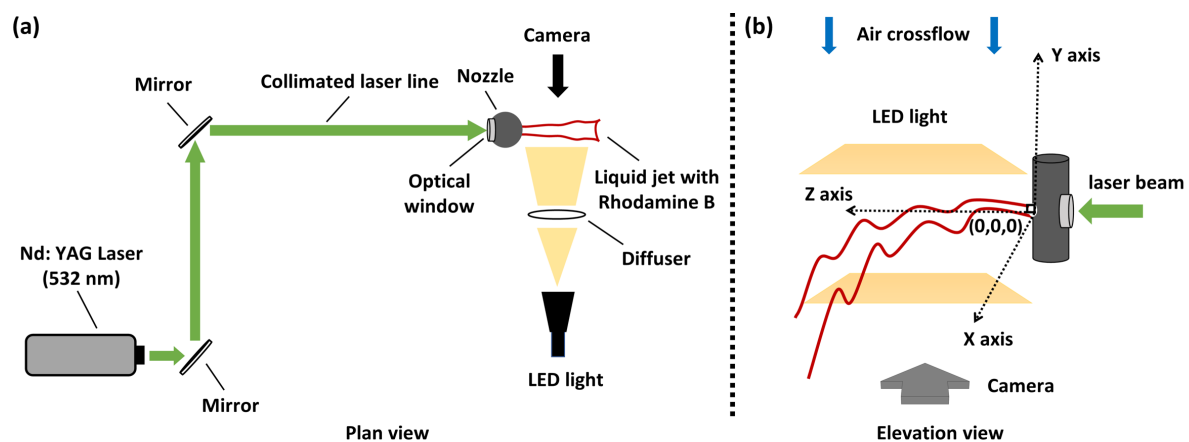


Fig. 3: Optical arrangements for the optical connectivity and shadowgraphy techniques; (a) plan view (b) elevation view.

2.3 Combined Optical Connectivity (OC) and Optical Flow Velocimetry (OFV)

The fluorescent intensity emitted from the liquid jet, as shown in **Fig. 4**, can be captured by OC which shows the instantaneous windward surface waves (the red windows in **Fig. 4**) and the stripping-off structures on the surface of liquid core (the black windows in **Fig. 4**). Since the fluorescent intensity variations indicates the surface locations of the wave structure or unsmooth liquid interface, the cross-correlation of the intensity distribution between subsequent images in time, similar to PIV algorithms, can be used to quantify the displacement of these local fluorescent intensity variations. This tracing approach is known as optical-flow velocimetry (OFV) or image correlation velocimetry (ICV), which has been applied to measure the velocity of variable scalar field, such as local flame and stripped-off droplets during atomisation (Georgios Charalampous & Hardalupas, 2016; Fielding, Long, Fielding, & Komiyama, 2001; Komiyama, Miyafuji, & Takagi, 1996; Sedarsky, Gord, Carter, Meyer, & Linne, 2009; Sedarsky, Idlahcen, Rozé, & Blaisot, 2013; Tokumaru & Dimotakis, 1995). For a liquid jet injected into a quiescent air, Wang and Hardalupas (2021) developed an hybrid OC-OFV method, combining the strength of both OC and OFV, to quantify the local interfacial liquid velocities by tracing the emitted fluorescent intensity from deformations of the liquid interface. In the context of LJIC, Ng et al. (2008) proposed a similar block tracing method to measure the velocity of the windward surface wave. The velocity of the windward surface wave was estimated by time-delayed image recordings from the double-pulsed shadowgraphy technique, which is also analogous to OFV method. However, while their approach can measure the windward interfacial velocity, the detailed stripping characteristics close to the nozzle exit or at the edge of the liquid core cannot be quantified by the shadowgraphy technique. Therefore, the combined OC and OFV technique (OC-OFV) of the present study is used to measure both the motions of windward surface waves and the stripping-off structures at the edge of the liquid core, and quantify instantaneous interfacial velocity vector maps of the LJIC. More details on OC-OFV can be found in Wang and Hardalupas (2021).

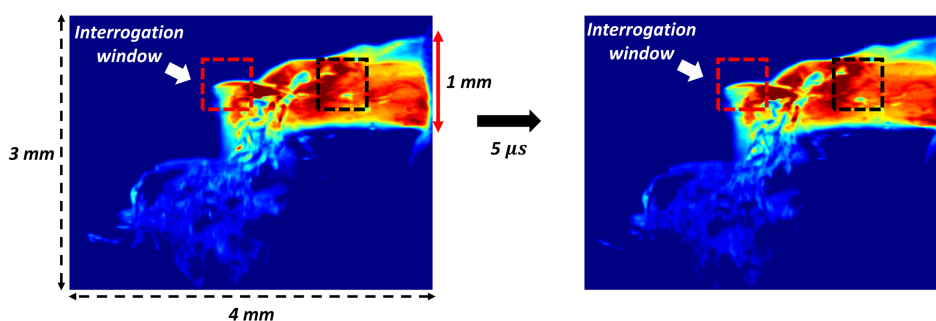


Fig. 4: Two OC fluorescent intensity images of the liquid jet in crossflow recorded by the camera with interval time $5\mu\text{s}$. Two example interrogation windows are shown on the images, which allow the application of Optical Flow Velocimetry (OFV) algorithms to measure the local velocity of the liquid interface structures.

The double pulse PIV laser operating at 532nm was used with interval time between the pulses of $5 \mu\text{s}$ for all flow cases of **Tab. 2** to generate time-delayed pairs of OC images. The fluorescent intensity in the interrogation window of **Fig. 4** was traced by a cross-correlation algorithm to calculate the displacement of the intensity pattern, which can then estimate the interfacial velocity on the liquid jet. The commercial PIV software (Davis 8) was used to compute the interfacial velocity and a multi-step cross-correlation algorithm was applied to the captured images. This algorithm used first a coarse interrogation window of 256×256 pixels with 50% window overlap to trace the movement of larger fluorescent intensity patterns. After capturing the movement of the larger scales, a refined interrogation window of 32×32 pixels with 75% window overlap is used to quantify the movement of the smaller scales that are present within the first interrogation window. Therefore, the smallest resolved flow structure is around $201.6 \mu\text{m}$, while adjacent velocity vectors have a separation distance of 8 pixels (around $50.4 \mu\text{m}$). A strict median filter and peak ratio were applied to reject spurious vectors. It is worth mentioning that a long interval time between the laser pulses is not recommended, since the geometry of the interfacial features may significantly change and the cross-correlation algorithm cannot identify the interfacial motion. Details of this cross-correlation algorithm can be found in Adrian & Raffel (2011; 2018).

OFV velocity measurements of the LJIC interfacial structures is based on 1500 pairs of OC fluorescent intensity images. Only flow cases with faster gas velocity (gas flow 3, 4 and 5) are analysed by OFV, since more surface deformations can be traced for these cases, particularly at the region close to the nozzle exit (see **Fig. 4**). In the current study, the OFV measurement was applied to the captured images with the coordinate system of **Fig. 4**. The axial component (parallel to Z axis) and transverse component (parallel to Y axis) of the instantaneous velocity vectors are defined as $u(t)$ and $v(t)$ respectively, and the corresponding mean axial velocity U and transverse velocity V can also be quantified. In addition, the current study only considered measurement locations with more than 150 valid vectors, in order to avoid the influence of the jet dynamics, scattering light and smooth surface. The maximum uncertainty of U and V is 4% at the location with evident surface deformation, which starts from $Z/D = 1$ along the jet surface. Before $Z/D = 1$, the maximum uncertainty can increase to 12 % at some locations due to the lack of generated deformed surface. All the uncertainties are estimated from the number of available vectors and 95% confidence interval.

3. Results and discussion

3.1 Images from OC and shadowgraphy techniques

Fig. 5 presents the OC fluorescent intensity and corresponding shadowgraphic images for all the flow cases of **Tab. 2** observed from the side-view. Shorter liquid jet penetration length can be observed with increasing We_G number for both techniques, and waves, possibly induced by R-T or K-H instabilities, are formed at the windward side of the liquid core. The bag and shear breakup features can be observed in the shadowgraphic images at the relevant breakup regime, which agrees with previous studies of LJIC (Mazallon et al., 1999; Ng et al., 2008; Sallam et al., 2004; Wu et al., 1997). Comparison between OC and shadowgraphic images shows that the surrounding droplet clouds and the stripped-off liquid clusters, as expected, are not recorded on the OC fluorescent intensity images. This is consistent with our previous studies when OC was applied to variable types of atomisation processes (Georgios Charalampous, Hadjiyiannis, & Hardalupas, 2016, 2019; G Charalampous et al., 2009; Hadjiyiannis, 2014).



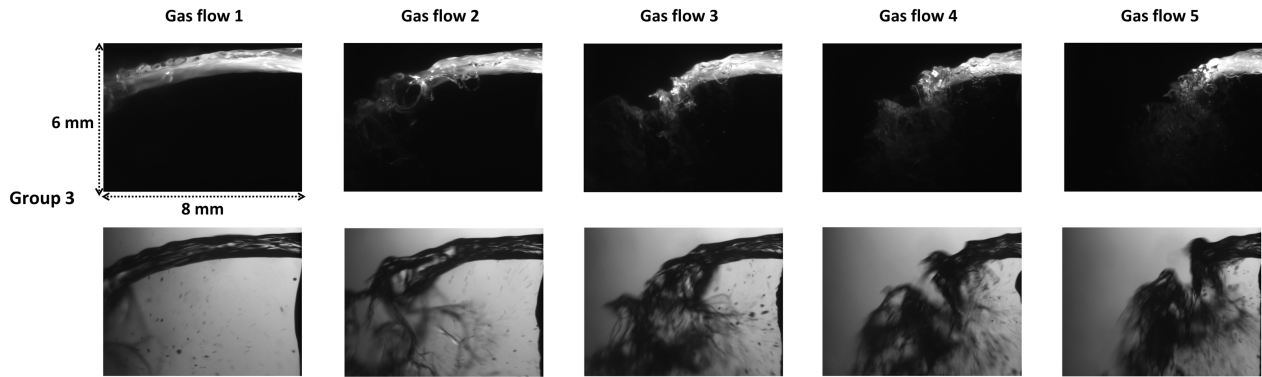
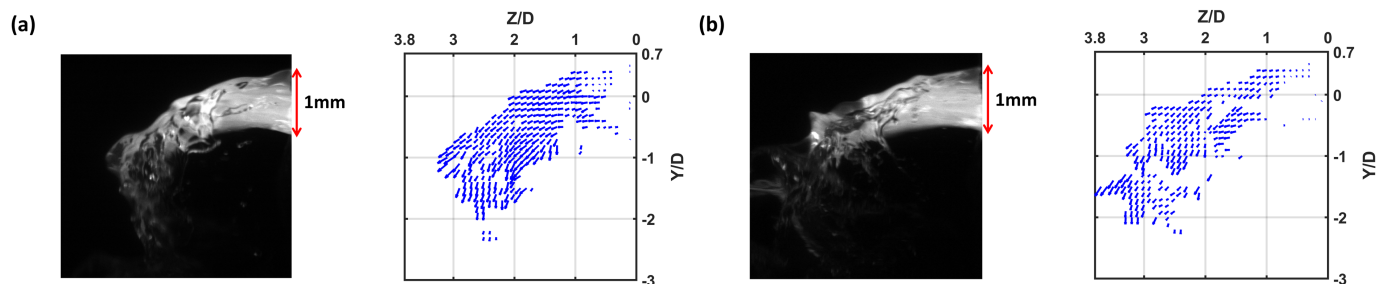


Fig. 5: OC fluorescent intensity images and shadowgraphic images for all flow cases of Tab. 2, the images from OC are plotted above the corresponding shadowgraphic image.

Meanwhile, the optical interference from the stripped-off liquid structures is not a severe problem for OC, even for atomisation under the shear breakup regime. Therefore, the laser light of the OC technique, escaping from the liquid core, is not capable to excite significant levels of fluorescence from the surrounding stripped-off liquid structures which demonstrates the OC advantage in measuring accurately the breakup features of LJIC, such as the breakup height and distance. It is noted that this verification is important, since the liquid jet is bending toward the gas flow and the liquid jet surface becomes wavy, which makes some of the laser light rays not being totally internally reflected on the liquid interface and escaping from the liquid core. Downstream of the complete liquid jet break in the gas flow, the light propagation in the liquid core stops and the light diffuses from the breakup point, which may excite fluorescence some of the droplets and induce low fluorescent intensity, which can be removed during image processing.

3.2 OC-OFV liquid interface velocity measurements

3.2.1 Interfacial motion of LJIC



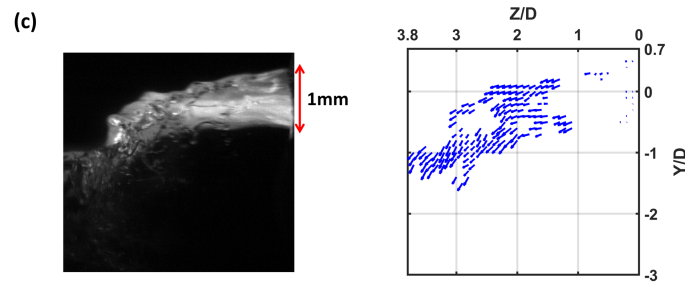


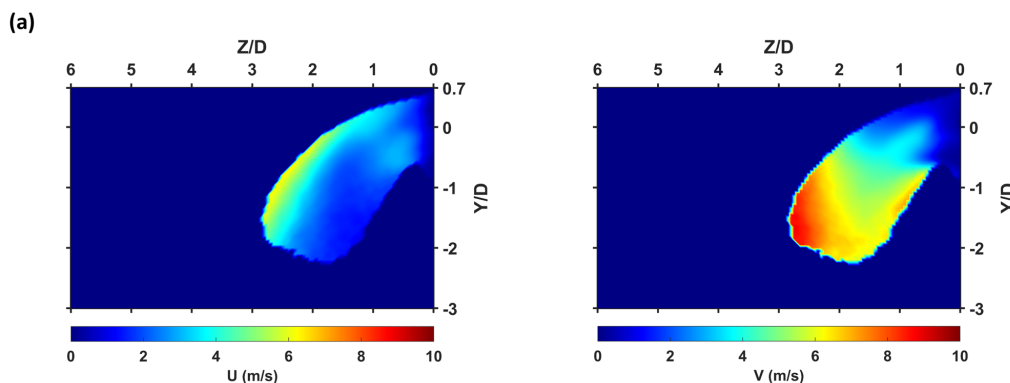
Fig. 6: Examples of the instantaneous velocity vector field and the corresponding OC intensity images. (a) Group 1, gas flow 3; (b) group 2, gas flow 4; (c) group 3, gas flow 5.

The interfacial velocity of the LJIC was computed by OFV as explained in Section 2.3. A large number of surface features were captured on the liquid jet surface after the nozzle exit, when the jet is exposed to high-speed gas flow, allowing OFV to measure both the motion of convective interfacial wave and stripping structures on the liquid jet surface. Velocity vectors calculated from the cross-correlation algorithm were decoupled to $u(t)$ and $v(t)$, which represents the velocity component associated with the liquid jet injecting direction (positive direction of Z axis) and gas flow direction (negative direction of Y axis) respectively. The instantaneous interfacial velocity $u(t)$ and $v(t)$ components were locally averaged as U and V to indicate the averaged interfacial motion on the surface, which are set positive when they are moving along the injection direction of the liquid jet and gas flow.

Examples of the measured instantaneous interfacial velocity vector fields for different flow cases are presented in **Fig. 6**. On the OC fluorescent intensity images, fluorescence with variable intensity can be observed on the jet surface due to the surface wrinkling. By tracing the fluorescent intensities, the movement of the large-scale windward wave and stripping structures at the jet surface can be both quantified and reflected on the vector map. The vector map shows that the vector at region with smooth surface was rejected by the strict peak ratio, since no variation of fluorescent intensity can be traced and thus no distinct peak can be found in the cross-correlation plate. Since the stripping surface structures do not have enough time to be formed immediately after the nozzle exit, the valid velocity vectors close to the nozzle exit are not as dense as at other regions due to the smooth surface. This characteristic is more evident for the jet of group 3, which has less velocity vectors close to the nozzle, since the higher liquid speed leads to a longer initial smooth surface after the nozzle exit. Besides, velocities of some stripping surface structures attaching on the leeward of the jet, such as the stretching ligaments, can also be detected by the OC-OFV technique.

The contour plots of the mean interfacial velocity U and V components are presented in **Fig. 7** for flow cases of gas flow 5 from each group of **Tab. 2**. The number of detected vectors at locations

right after the nozzle exit ($Z/D < 0.5$) is not enough to provide a mean velocity with low uncertainty since the jet surface is smooth and only limited surface structures can be recorded. The statistical uncertainties at these regions increase to 10% relative to that away from the nozzle, which is lower than 5% for a 95% confidence interval. **Fig. 7** shows that velocity component U on the windward side of the liquid jet is higher than at the other region and has a strong tendency to increase with distance from the nozzle, especially when the jet starts bending towards the gas flow direction. In addition, the value of U at $Z/D = 1.5$ increases from group 1 (**Fig. 7(a)**) to group 3 (**Fig. 7(c)**). As the liquid jet is gradually deflected by the gas flow, the computational work of Li and Soteriou (2016) and PIV measurement of Elshamy et al. (2006), show that the velocity of the deflected gas flow close to the jet surface has initially lower magnitude close to the nozzle exit and increases gradually with the level of bending of the liquid jet and eventually approaches the freestream gas velocity when the liquid jet is fully aligned to the gas flow. Hence, the characteristics of the U velocity component on the windward are expected, since the injection liquid jet velocity U_L increases from group 1 to 3, and the near surface faster gas flow on the windward side also accelerates the windward interfacial velocity of the liquid jet through aerodynamic shear especially as the liquid jet aligns to the gas flow direction. Moreover, with downstream distance from the nozzle, the U component at the edge and leeward of the jet gradually decreases due to the momentum exchange with the local gas flow. It is noted that the velocity measurements from OC-OFV provide the motion on the 3-D circumference of the jet interface rather than a 2-D observation plane. Therefore, the kinematic characteristics at different regions of the jet surface must be coupled with the 3-D interface geometry.



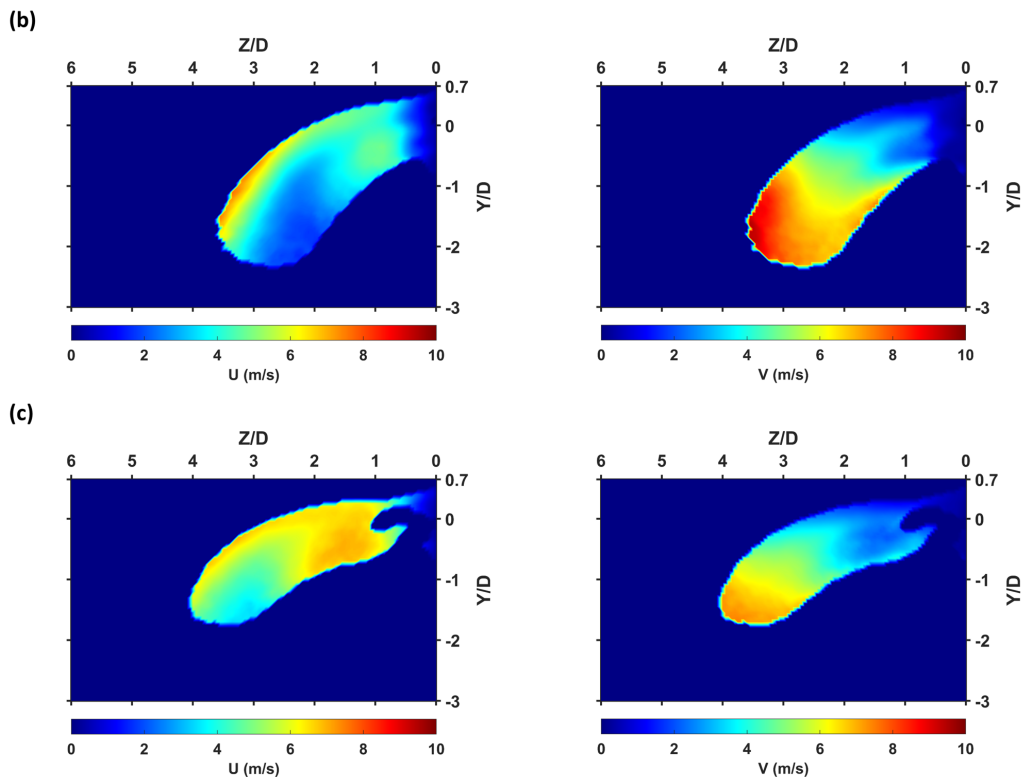


Fig. 7: Contour plots of mean interfacial velocity U (left) and V (right) components. (a) Group 1, gas flow 5; (b) group 2, gas flow 5; (c) group 3, gas flow 5.

The V velocity component, shown in **Fig. 7**, initiates from an almost zero magnitude at the windward side, since the liquid jet is injected perpendicularly to the gas flow and the V component is zero close to the nozzle exit. Then, the V component increases downstream mainly due to jet deflection due to the interaction with the high-speed gas flow. The gaseous shear force surrounding the liquid jet induces a V component to jet surface structures and the aerodynamic drag may also contribute to the V component of stripping structures with large dimensions. Therefore, near the tail of the liquid jet, as expected, a higher V is observed due to the more durable gas acceleration. The maximum value of V can be found at the front tip of the liquid jet surface, which may indicate that the gas velocity is higher at this region and the surface structures, therefore, are accelerated further. Therefore, the combined OC-OFV technique is capable of quantifying the interfacial movement of LJIC and explain the development of the interfacial motion of the liquid jet for the first time.

The interfacial velocity components on the windward side of the LJIC, from now on, are decomposed into two components U_W and V_W , as shown in **Fig. 8**. The windward velocity U_W and V_W refer to the U and V velocity component at the windward side of the liquid jet, indicating the movement of the instability waves or the surface structures at the windward side. The windward

velocity results from the interaction between the local gas and liquid flow on the windward jet interface, where gaseous shear is imposed on the liquid surface due to the deflected fast gas flow attaching on the windward side of the liquid jet, which is moving slower than V_G before the jet is aligned to the gas flow direction, and gradually accelerating the liquid interfacial velocity on the windward side of the jet. The uncertainty of the presented windward velocity components is less than 6.3% with 95% confidence interval.

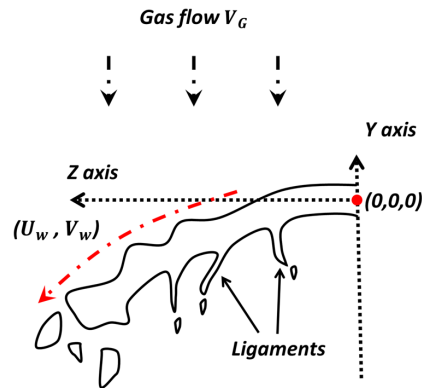


Fig. 8: Schematic of the behaviour of the windward interfacial velocity components.

The U component of the windward velocity, U_W , for different flow conditions of each group of **Tab. 2** is shown in **Fig. 9**. The value of U_W is measured after the nozzle exit and the initial U_W at $Z/D = 0$ is close to zero, due to the liquid boundary layer formed on the nozzle wall before the exit. After the liquid exits the nozzle, the free liquid surface changes due to the liquid shear layer relaxation induced by the internal viscous force associated with the sharp velocity gradient under the liquid interface. A sharp acceleration of U_W , hence, can be observed approximately before $Z/D = 1$ for all flow cases. The magnitude of U_W at $Z/D = 1$ is larger for the group with a higher U_L (increases from group 1 to 3) and the value of U_W approaches the corresponding injection velocity U_L . Hence, owing to the nozzle length with $L/D = 1.5$, the boundary layer of the liquid jet at the nozzle exit is thin and forms an initial velocity deficit close to the nozzle exit. The liquid velocity acceleration should also be affected by the attaching fast gas flow on the surface at the region before $Z/D = 1$.

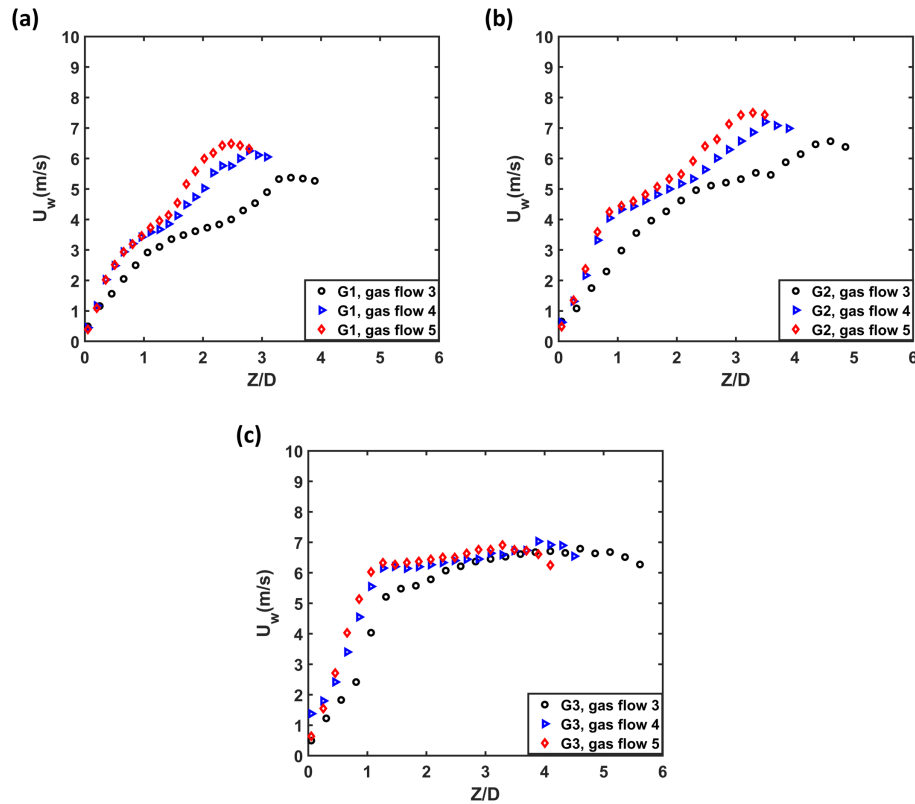


Fig. 9: U component of the windward velocity (U_W) for different flow cases of **Tab. 2**. (a) Flow cases of group 1; (b) flow cases of group 2; (c) flow cases of group 3.

Meanwhile, a secondary effect appears to influence the acceleration of U_W after $Z/D = 1$, indicating that the high-speed gas flow on the windward side becomes the main accelerating influence of the jet interface after the viscous force in the liquid shear layer is reduced due to the relaxation of the layer. The development of the U_W along the surface of the jet after around $Z/D = 1$ is mainly determined by the speed of gas flow. U_W for flow cases with faster gas flow is larger and grows faster than the other cases, which is more evident for the cases of groups 1 and 2. This also interprets the slightly stronger growing trend of U_W further away from the nozzle exit (see the profiles after $Z/D = 2$ in **Fig. 9(a)** and **(b)**), since the jet at this region is further bending toward the gas flow direction and an increased gas flow shear is generated on the windward surface due to the faster attaching gas flow. For the flow cases of group 3 (**Fig. 9(c)**), the secondary increasing trend of U_W is not obvious as for the other groups, since the bending of the liquid jet is not distinct which results to a mild gas flow shear. Besides, U_W gradually ceases to grow and becomes constant towards the end of the velocity profile. At this region, the jet approaches breakup, and the tail of the jet interface is almost parallel to the gas flow. The gas flow shear, hence, mainly accelerates the V component of windward velocity rather than the U component at this region.

The currently presented variable U_W values with distance from the nozzle do not support the

measurements of Ng et al. (2008) and Sallam et al. (2004), who considered that U_W remains equal to U_L at downstream distances from the nozzle. In their experiment, the measurement of U_W was based on double-pulsed shadowgraphic technique and traced the movement of the windward instability wave. The difference between the two measurements is possibly explained by the different types of injection nozzle. The nozzle used by Ng et al. (2008) and Sallam et al. (2004) was a supercavitating nozzle, and thus the initial interfacial velocity may not be influenced by the liquid flow boundary layer at the nozzle wall. In addition, the measurement from their shadowgraphic technique cannot track the development of the interfacial velocity during the entire primary breakup process as the OC-OFV can and leads to U_W measured as being approximately constant, which is avoided by the OC-OFV technique.

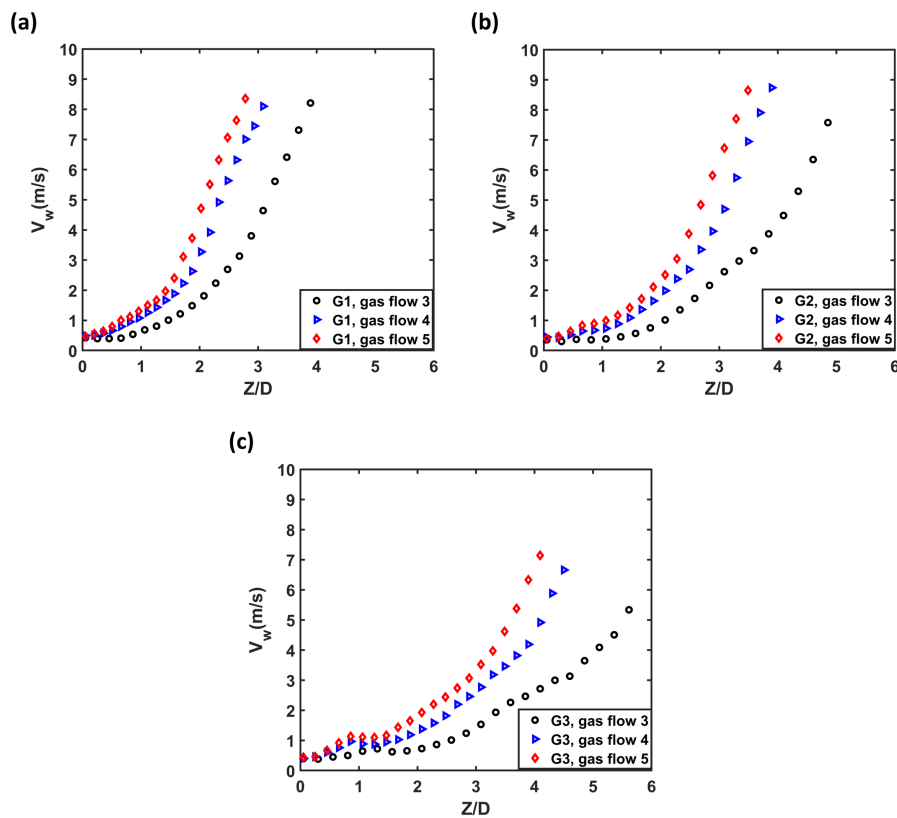


Fig. 10: V component of the windward velocity (V_W) for different flow cases of **Tab. 2**. (a) Flow cases of group 1; (b) flow cases of group 2; (c) flow cases of group 3.

The V component of windward interfacial velocity V_W is presented in **Fig. 10**, which allows comparison with the variation of the U component of **Fig. 9**. Similarly as for the U_W , V_W has a small magnitude with almost 0 m/s close to the nozzle exit, since the initial liquid jet has no velocity component along the Y axis. The measured small initial value of V_W must have been induced by the acceleration from the high-speed gas flow. Moreover, the acceleration of V_W with distance from

the nozzle is not linear but follows a parabolic growth. This characteristic of V_W is consistent with the deflection of the liquid jet, since the acceleration due to the high gas flow shear increases both U_W and V_W , and the further bending of the liquid jet induced stronger shear that accelerates faster the V component. Meanwhile, close to the tail of the liquid jet, the growing trend of V_W becomes more evident due to the described mechanisms, which are also causing the nearly constant U_W values at the tail of the jet, shown in **Fig. 9**. For flow conditions of the same group, the flow case with faster gas flow has a steeper growth trend in **Fig. 10**. This can be explained by the higher gas flow shear which accelerates the liquid jet surface but also bends it earlier. The stronger penetration of the liquid jets with higher U_L delays the rapid growth of V_W due to delayed jet deflection, resulting to lower V_W values at the same location compared to the liquid jet with lower U_L for the same gas flow. In general, results from U_W and V_W manifest the development of the windward motion on the liquid jet, demonstrating the interfacial interaction of the two-phase flow. The local geometry of the liquid jet also influences the shear and relevant momentum exchange between the gas and liquid phase.

4. Conclusions

The current study conducted a liquid jet in cross-flow (LJIC) experiment that was operated with different gas Weber number and liquid-to-gas momentum flux ratio conditions leading to different breakup regimes, including bag, multimode, and shear breakup regimes. Both shadowgraphy and optical connectivity (OC) techniques were utilized to capture the liquid jet geometry during the primary breakup process, which demonstrated the potential advantages of OC in measuring accurately the breakup characteristics and the liquid jet surface features.

Combined Optical Connectivity and Optical Flow Velocimetry (OC-OFV) technique was applied to measure the interfacial velocity vector of the circumferential surface structures of the LJIC. This experiment, for the first time, quantified the detailed spatial distribution of the interfacial velocity on surface of the continuous liquid core in high-speed gaseous crossflow. The results show that the development of the interfacial velocity at the windward side is associated with the deflection of the liquid jet by the gas cross-flow. The interaction of the liquid jet trajectory with the local gas velocity close to the surface generates different degrees of gas shear on the windward side of the liquid jet, which determines the spatial development of two components of the interfacial velocity associated with different liquid surface structures. Besides, the interfacial velocity may indicate the initial velocity of stripped liquid plumes or droplets from different locations of the jet surface

during primary breakup and explain the distribution of downstream spray droplets during the secondary breakup.

References

- Adrian, L., Adrian, R. J., & Westerweel, J. (2011). Particle image velocimetry: Cambridge university press.
- Arienti, M., & Soteriou, M. C. (2009). Time-resolved proper orthogonal decomposition of liquid jet dynamics. *Physics of Fluids*, 21(11), 112104.
- Behzad, M., Ashgriz, N., & Karney, B. (2016). Surface breakup of a non-turbulent liquid jet injected into a high pressure gaseous crossflow. *International Journal of Multiphase Flow*, 80, 100-117.
- Birouk, M., Azzopardi, B. J., & Stähler, T. (2003). Primary Break - up of a Viscous Liquid Jet in a Cross Airflow. *Particle & Particle Systems Characterization: Measurement and Description of Particle Properties and Behavior in Powders and Other Disperse Systems*, 20(4), 283-289.
- Broumand, M., & Birouk, M. (2016). Liquid jet in a subsonic gaseous crossflow: Recent progress and remaining challenges. *Progress in Energy and Combustion Science*, 57, 1-29.
- Broumand, M., & Birouk, M. (2019). Liquid jet primary breakup in a turbulent cross-airflow at low Weber number. *Journal of Fluid Mechanics*, 879, 775-792.
- Charalampous, G., Hadjiyiannis, C., & Hardalupas, Y. (2016). Comparative measurement of the breakup length of liquid jets in airblast atomisers using optical connectivity, electrical connectivity and shadowgraphy. *Measurement*, 89, 288-299.
- Charalampous, G., Hadjiyiannis, C., & Hardalupas, Y. (2019). Proper orthogonal decomposition of primary breakup and spray in co-axial airblast atomizers. *Physics of Fluids*, 31(4), 043304.
- Charalampous, G., & Hardalupas, Y. (2016). How do liquid fuel physical properties affect liquid jet development in atomisers? *Physics of Fluids*, 28(10), 102106.
- Charalampous, G., Hardalupas, Y., & Taylor, A. (2007). A novel technique for measurements of the intact liquid jet core in a coaxial airblast atomizer. Paper presented at the 45th AIAA Aerospace Sciences Meeting and Exhibit.
- Charalampous, G., Hardalupas, Y., & Taylor, A. (2009). Novel technique for measurements of continuous liquid jet core in an atomizer. *AIAA Journal*, 47(11), 2605-2615.
- Elshamy, O., Tambe, S., Cai, J., & Jeng, S.-M. (2006). Structure of liquid jets in subsonic crossflow at elevated ambient pressures. Paper presented at the 44th AIAA Aerospace Sciences Meeting and Exhibit.

Fielding, J., Long, M. B., Fielding, G., & Komiyama, M. (2001). Systematic errors in optical-flow velocimetry for turbulent flows and flames. *Applied Optics*, 40(6), 757-764.

Ghosh, S., & Hunt, J. (1998). Spray jets in a cross-flow. *Journal of Fluid Mechanics*, 365, 109-136.

Hadjiyiannis, C. (2014). Investigation of break-up process of liquids and downstream spray characteristics in air-blast atomisers. PhD thesis. Imperial College London.

Kelso, R. M., Lim, T., & Perry, A. (1996). An experimental study of round jets in cross-flow. *Journal of Fluid Mechanics*, 306, 111-144.

Komiyama, M., Miyafuji, A., & Takagi, T. (1996). Flamelet behavior in a turbulent diffusion flame measured by Rayleigh scattering image velocimetry. Paper presented at the Symposium (International) on Combustion.

Lee, K., Aalburg, C., Diez, F. J., Faeth, G. M., & Sallam, K. A. (2007). Primary breakup of turbulent round liquid jets in uniform crossflows. *AIAA Journal*, 45(8), 1907-1916.

Li, X., & Soteriou, M. C. (2016). High fidelity simulation and analysis of liquid jet atomization in a gaseous crossflow at intermediate Weber numbers. *Physics of Fluids*, 28(8), 082101.

Li, X., & Soteriou, M. C. (2018). Detailed numerical simulation of liquid jet atomization in crossflow of increasing density. *International Journal of Multiphase Flow*, 104, 214-232.

Linne, M. A., Paciaroni, M., Gord, J. R., & Meyer, T. R. (2005). Ballistic imaging of the liquid core for a steady jet in crossflow. *Applied Optics*, 44(31), 6627-6634.

Lubarsky, E., Reichel, J. R., Zinn, B. T., & McAmis, R. (2010). Spray in crossflow: Dependence on Weber number. *Journal of engineering for gas turbines and power*, 132(2).

Lubarsky, E., Shcherbik, D., Bibik, O., Gopala, Y., & Zinn, B. (2012). Fuel jet in cross flow—experimental study of spray characteristics. *Advanced Fluid Dynamics*, 59.

Mahesh, K. (2013). The interaction of jets with crossflow. *Annual review of fluid mechanics*, 45, 379-407.

Mazallon, J., Dai, Z., & Faeth, G. (1999). Primary breakup of nonturbulent round liquid jets in gas crossflows. *Atomization and Sprays*, 9(3).

Ng, C.-L., Sankarakrishnan, R., & Sallam, K. (2008). Bag breakup of nonturbulent liquid jets in crossflow. *International Journal of Multiphase Flow*, 34(3), 241-259.

Osta, A., & Sallam, K. (2007). Effect of nozzle length/ diameter ratio on the breakup of liquid jets in crossflow. *APS*, 60, GC. 003.

Raffel, M., Willert, C. E., Scarano, F., Kähler, C. J., Wereley, S. T., & Kompenhans, J. (2018). *Particle image velocimetry: a practical guide*: Springer.

Sallam, K., Aalburg, C., & Faeth, G. (2004). Breakup of round nonturbulent liquid jets in gaseous crossflow. *AIAA Journal*, 42(12), 2529-2540.

- Sallam, K., Dai, Z., & Faeth, G. (2002). Liquid breakup at the surface of turbulent round liquid jets in still gases. *International Journal of Multiphase Flow*, 28(3), 427-449.
- Sallam, K., Ng, C., Sankarakrishnan, R., Aalburg, C., & Lee, K. (2006). Breakup of turbulent and non-turbulent liquid jets in gaseous crossflows. Paper presented at the 44th AIAA Aerospace Sciences Meeting and Exhibit.
- Sedarsky, D., Gord, J., Carter, C., Meyer, T., & Linne, M. (2009). Fast-framing ballistic imaging of velocity in an aerated spray. *Optics Letters*, 34(18), 2748-2750.
- Sedarsky, D., Idlahcen, S., Rozé, C., & Blaisot, J.-B. (2013). Velocity measurements in the near field of a diesel fuel injector by ultrafast imagery. *Experiments in fluids*, 54(2), 1451.
- Seuntiëns, H., Kieft, R., Rindt, C., & Van Steenhoven, A. (2001). 2D temperature measurements in the wake of a heated cylinder using LIF. *Experiments in Fluids*, 31(5), 588-595.
- Tokumar, P., & Dimotakis, P. (1995). Image correlation velocimetry. *Experiments in Fluids*, 19(1), 1-15.
- Wang, T., & Hardalupas, Y. (2021). Combined Optical Connectivity and Optical Flow Velocimetry for interfacial characterisation of liquid atomisation. Paper presented at the International Conference on Liquid Atomization and Spray Systems (ICLASS).
- Wu, P.-K., Kirkendall, K. A., Fuller, R. P., & Nejad, A. S. (1997). Breakup processes of liquid jets in subsonic crossflows. *Journal of Propulsion and power*, 13(1), 64-73.
- Wu, P.-K., Kirkendall, K. A., Fuller, R. P., & Nejad, A. S. (1998). Spray structures of liquid jets atomized in subsonic crossflows. *Journal of propulsion and power*, 14(2), 173-182.